

## Development of a Fine Digital Sun Sensor for STSAT-2

**Sung-Ho Rhee\* and Joon Lyou\*\***

*Satellite Technology Research Center, KAIST, Daejeon 305-701, Korea*

*Department of Electronics Engineering, Chungnam National University, Daejeon 305-764, Korea*

### Abstract

Satellite devices for fine attitude control of the Science & Technology Satellite-2 (STSAT-2). Based on the mission requirements of STSAT-2, the conventional analog-type sun sensors were found to be inadequate, motivating the development of a compact, fast and fine digital sun sensor (FDSS). The FDSS uses a CMOS image sensor and has an accuracy of less than 0.03degrees, an update rate of 5Hz and a weight of less than 800g. A pinhole-type aperture is substituted for the optical lens to minimize its weight. The target process speed is obtained by utilizing the Field Programmable Gate Array (FPGA), which acquires images from the CMOS sensor, and stores and processes the image data. The sensor accuracy is maintained by a rigorous centroid algorithm. This paper describes the FDSS designs, realizations, tests and calibration results.

**Key words:** STSAT-2, FDSS, CMOS-image sensor(CIS), Pinhole-type aperture, Centroid algorithm

### 1. Introduction

An attitude determination system for satellites is developed by using the data measured by attitude sensors, such as the sun sensor (SS), earth horizon sensor (EHS), magnetometer (MAG), fiber optic gyro (FOG) and star tracker (ST). Among these sensors, the sun sensors especially have been used widely to determine coarse and fine attitudes. Analog-type sun sensors have been developed for Korea Institute Technology Satellite (KITSAT)-1, 2, 3 and Science & Technology Satellite-1 (STSAT-1) over the past decade. These analog sun sensors have an accuracy of less than 1 degree.

Based on the mission requirements of STSAT-2, the conventional analog-type sun sensors were found to be inadequate, motivating the development of a compact, fast and fine digital sun sensor (FDSS) [1,2]. The main objective of the FDSS is precise attitude determination of STSAT-2 for precision sun pointing missions and new major technology development projects. The target process speed is obtained

by utilizing the Field Programmable Gate Array (FPGA), which acquires images from the CMOS sensor, and stores and processes the image data. The Field Of View (FOV) is 20×20 degrees for each axis. The sensor accuracy is maintained by a rigorous centroid algorithm. FDSS mounted on STSAT-2 is shown in Fig.1. Table 1. shows the specifications of FDSS

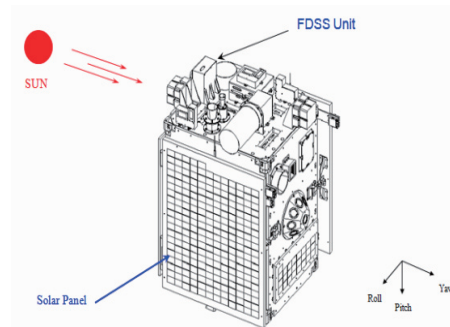


Fig. 1. FDSS mounted on STSAT-2

This is an Open Access article distributed under the terms of the Creative Commons Attribution Non-Commercial License (<http://creativecommons.org/licenses/by-nc/3.0/>) which permits unrestricted non-commercial use, distribution, and reproduction in any medium, provided the original work is properly cited.

© \* Author  
E-mail: shrhee@satrec.kaist.ac.kr Tel:+82-42-867-2966  
\*\* Corresponding author  
E-mail: jlyou@cnu.ac.kr Tel:+82-42-821-5669

Table 1. Specifications of FDSS

Item	Specification	Remark
Field of View	20° x 20°	
Accuracy	< 0.03° (2σ)	2-axis
Weight	< 1kg	
Power	1.5W@normal	
Operation LifeTime	>2 years	
Size	150x150x 160	mm <sup>3</sup>

## 2. Optical Design of FDSS

### 2.1 Basic principles of FDSS

The basic principles of the FDSS are as follows. Sunlight passes through the aperture of the FDSS and is projected onto the surface of the CMOS image sensor. Each pixel of the CMOS image sensor converts the projected sunlight into 10-bit digital signals. These signals are stored by the FPGA, which generates and controls the 10-bit digital signals. The Micro Processor Unit (MPU) reads the stored data from the FPGA, calculates the entrance degree of the sunlight ray, and provides the calculated entrance degrees to the On-Board Computer (OBC), which determines the attitude and processes the control program. The FDSS is divided into three parts, as shown in Fig. 2. The first part is the optical part: sunlight passes through aperture, is attenuated by the Neutral Density Filter (NDF) and filtered by the Band Pass Filter (BPF). The optical part projects the sunlight onto the surface of the CMOS image sensor. The second part is the FPGA part: this part generates the control signals and sends these signals to the CMOS image sensor. The

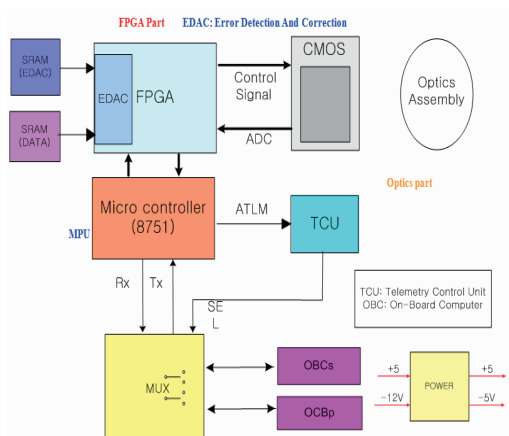


Fig. 2. FDSS electrical scheme.

second part stores the data acquired from the CMOS image sensor and communicates with the micro process unit (MPU) by using data packets. The third part is the MPU: it communicates with the OBC and calculates the incident angle of the sunlight using the centroid algorithm.

### 2.2 Optical part of FDSS

Fig. 3 describes the schematic of the optical part on the FDSS. The sunlight enters the aperture with the radius of  $\rho$  is filtered by the NDF, and attenuated by the BPF. The optical part is coated internally with an anti-reflection material to minimize the reflection of the sunlight. Also, the optics and mechanical structures need to be accurately aligned between the aperture and the CMOS image sensor. When the CIS is mounted on the printed circuit board (PCB), the CIS is aligned with reference to the outline of the CIS on the PCB.

### 2.3 Diffraction characteristics of the aperture

The characteristics of the sunlight on the surface of the CMOS image sensor need to be analyzed in the optical system. Particularly, the intensity of the sunlight must be decreased to prevent it from exceeding the allowable electrical threshold of the CMOS image sensor. After considering the diffraction effect, a stable wavelength is chosen for the BPF.

The optical characteristics of the FDSS and the distribution of the sunlight energy need to be considered for the detection of the incident angle.

$$\vec{E} = \epsilon_A \frac{e^{i(\omega t - kR)}}{R} \iint e^{ik(Yy + Zz)} dS \quad (1)$$

$$z = \rho \cos \phi, y = \rho \sin \phi, Z = q \cos \Phi, Y = q \sin \Phi, \quad (2)$$

$$I = \int_{\rho=0}^a \int_{\phi=0}^{2\pi} e^{i(k\rho q/R)\cos(\phi-\Phi)} \rho d\rho d\phi \quad (3)$$

where  $\epsilon_A$  is the permittivity of the air;  $k$  is the  $k$  is the  $2\pi/\lambda$ ;

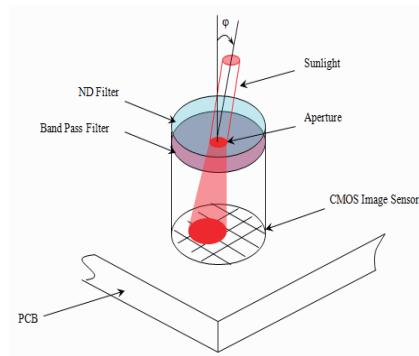


Fig. 3. The schematic of the aperture for the FDSS.

the  $t$  is the time ; the  $\omega$  is the  $2\pi f$ .

That  $I(q)$  is twice as long as the diameter of the aperture in length.

Because of  $I \propto E^*E$ , the intensity,  $I$ , is given by Eq. (4) as follows [3].

$$I = I_0 \left| \frac{J_1(kaq/R)}{kaq/R} \frac{J_1(kbq/R)}{kbq/R} \right|^2 \tag{4}$$

where  $a$  is the radius of the aperture;  $b$  is the maximum symmetric distance of the aperture through which the sunlight passes ;  $\Phi$  is the rotation angle on the  $y$ - $z$  plane about the  $z$  axis; and  $q$  is the distance between the center and the diffraction pattern.

$I_{tot}$  is the total energy which is received from the a circular aperture. The energy is

$$I(q) = I_{tot} / \int_0^{\pi} \int_0^{2\pi} \left[ \frac{J_1(kaq/R)}{kaq/R} \frac{J_1(kbq/R)}{kbq/R} \right]^2 q dq d\theta \tag{5}$$

Eq. (5) shows that  $I(q)$  becomes zero when  $q=116\mu\text{m}$ . This illustrates the fact that  $I(q)$  is twice as long as the diameter of the aperture in length.

Fig. 5 displays the diffraction distance of the aperture. The ratio of the first diffraction pattern and the total diffraction energy is calculated as follows

$$I(q_0) = \int_0^{0.000116} \int_0^{2\pi} I(q) q dq d\theta / \int_0^{\pi} \int_0^{2\pi} I(q) q dq d\theta \tag{6}$$

Eq. (6) shows that most energies concentrate within the first circular diffraction ( $q_0$ ) pattern. The CMOS image sensor has  $512 \times 512$  pixels

The pixel efficiency is approximately 7%. When the pixels are at a right angle to the sunlight, the energy distribution of the sunlight by the diffraction effect and the allocation of the sunlight energy are calculated as follows.

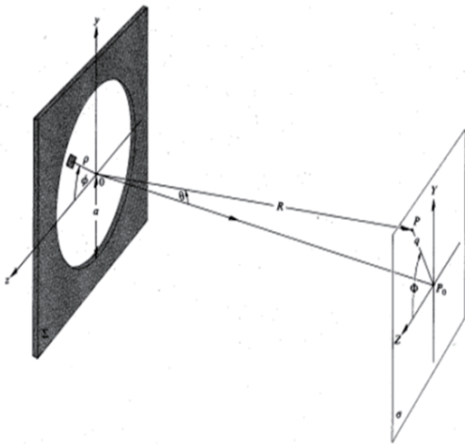


Fig. 4. Angular size of the sunlight.

Eq. (4) uses the Cartesian coordinate system. Therefore, Eq. (4) needs to be changed as follows

$$I(y,z) = I_0 \left[ \frac{J_1(ka\sqrt{y^2+z^2}/R)}{ka\sqrt{y^2+z^2}/R} \frac{J_1(kb\sqrt{y^2+z^2}/R)}{kb\sqrt{y^2+z^2}/R} \right]^2 \tag{7}$$

where  $I_0 = 487.4$

Based on Eq. (7), the energy radiated into the central pixel for 0.1 second is

$$E_{0,0} = 0.007 \times \int_{-12.5\mu\text{m}}^{12.5\mu\text{m}} \int_{-12.5\mu\text{m}}^{12.5\mu\text{m}} I(y,z) dy dz = 1.29E-10J \tag{8}$$

Using Eq. (8), the locations of the other pixels close to the center pixels can be calculated. The first airy disk is plotted by the pixels, as shown in Fig. 5.

Electrons are generated by the photo effect. The energy of an electron is

$$h\nu = 6.626E-34 \times (3E8/880E-9) = 0.2259E-18(J) \tag{9}$$

Eqs. (10) and (11) can be used to calculate the number of electrons generated.

$$N(E_{0,0}) = 5.72E8(ea) \tag{10}$$

$$N(E_{2,0}) = 2.65E8(ea) \tag{11}$$

We designed a filter for the attenuation of the sunlight. The sunlight's intensity needed to be decreased by using the NDF because the intensity was too strong. Using the above results, Eq. (12) shows the percentage of attenuation that a filter would need to achieve.

$$(311,000 / 5.72E8) \times 100 = 0.0544 \tag{12}$$

A 5.44% filter has to be used. If the transmittance of

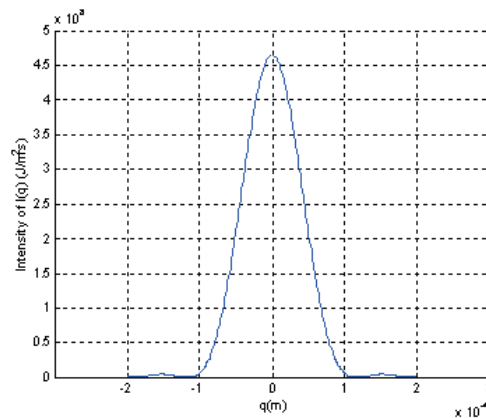


Fig.5.  $I(q)$  graph

the NDF is low, the S/N characteristics of the CIS tend to decrease. Therefore, there needs to be a trade-off between the NDF and BPF to obtain the optimal performance [4]. An appropriate exposure time and sampling time are also chosen by the designer. Also the developer should consider the stability of the MPU and the FPGA

### 3. Calculation algorithm for the incident angle

The center of the aperture, through which the sunlight passes at an incident angle, must be found. For this purpose, a sunlight image was projected onto the pixels of the CMOS image sensor. Among the several algorithms that can be used to find the center, the centroid algorithm is well-known and popular, given as Eq. (13).

Fig. 6 shows the size of the CMOS sensor. X and Y are the center coordinates calculated by the centroid algorithm. The incident angle error of the sunlight was simulated, and the maximum error was less than 2.0E-4degrees.

$$X = \frac{\sum_{j=1}^n \sum_{i=1}^m j \cdot I_{ij}}{\sum_{j=1}^n \sum_{i=1}^m I_{ij}} \quad Y = \frac{\sum_{j=1}^n \sum_{i=1}^m i \cdot I_{ij}}{\sum_{j=1}^n \sum_{i=1}^m I_{ij}} \quad (13)$$

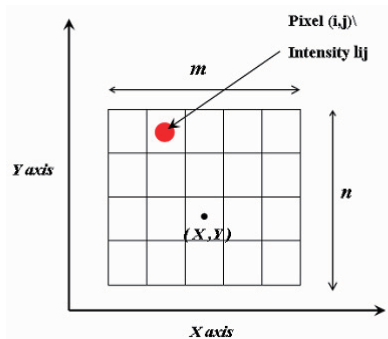


Fig. 6. Coordinate calculated by the centroid algorithm.

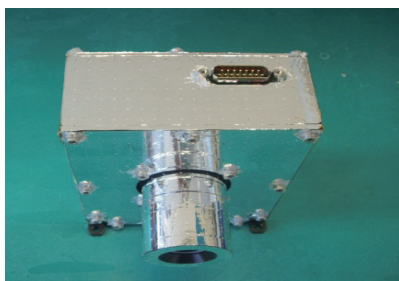


Fig.7. FDSS made by SaTReC

i, j : Number of pixels.

I : Intensity of each pixel.

The incident angles of the sunlight to the x-axis and y-axis are  $\alpha$  and  $\beta$ , respectively, given by Eqs. (14) and Eq. (15) as follows [5, 6].

$$\alpha = \tan^{-1} \frac{X}{h} (^{\circ}) \quad (14)$$

$$\beta = \tan^{-1} \frac{Y}{h} (^{\circ}) \quad (15)$$

h : the height between the CMOS image sensor and the aperture.

X : distance of the pixel on x axis.

Y : distance of the pixel on y axis.

Fig. 7 is a photo of the developed FDSS for FM. It has been prepared for use in space. It is coated for thermal control.

### 4. FDSS Measurement Results

#### 4.1 Measurement facility

The test facility for calibration consists of the solar simulator, a 2-axis rotary stage, and a collimator in the Satreci optical room. The solar simulator has AM1.5 precision, and the 2 axis rotary stage has 1/1000mm resolution accuracy [7].

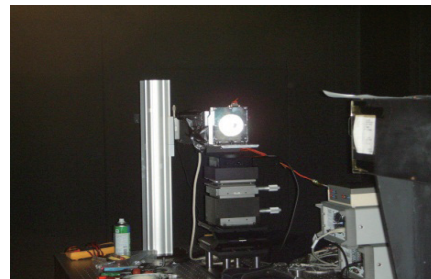


Fig. 8. Calibration facility for the FDSS

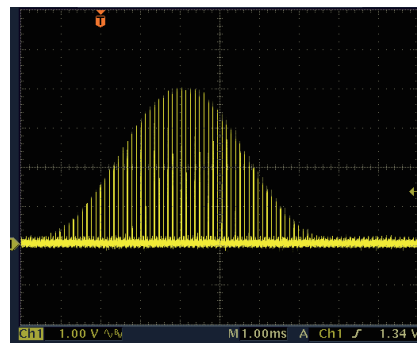


Fig. 9. Waveform of the CIS output

Fig. 8 shows the calibration facility of SI (SaTReC Initiative) for the FDSS.

#### 4.2 Signal of the CIS output

Fig. 9 shows the signal of CIS when the sunlight enters to the pin hole. This wave is similar to the analyzed waveform. This waveform is suitable for the application of the algorithm. Fig. 10 shows the graph of the errors versus the x-axis when the horizon axis degree is zero. The error range is within the accuracy of the 0.03 degrees [7].

Based on the results, the target accuracy can be obtained. Also Fig. 10 shows the graph of the errors versus the y-axis when the horizon axis degree is zero. The algorithm is very important for obtaining accurate and best performance.

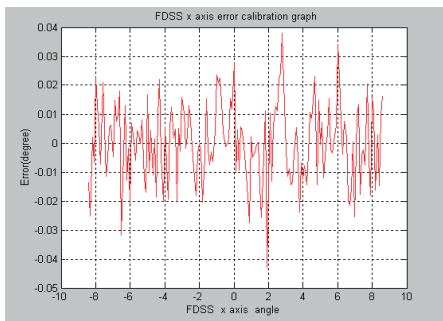


Fig.10. FDSS x-axis error result with zero degree

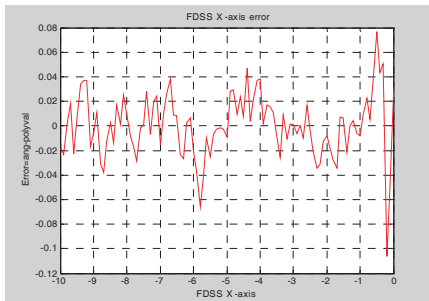


Fig. 11. FDSS y-axis error result with zero degree

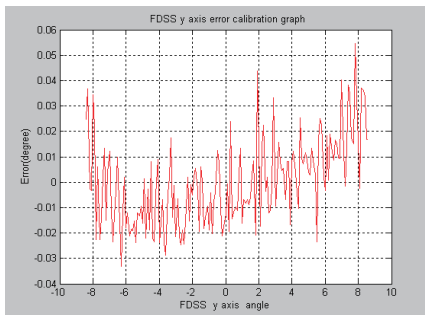


Fig. 12. FDSS -x-axis error result with +45 degree rotation.

Therefore, better algorithms need to be studied for high-level, fine digital sensors.

Table 2 provides the measurement errors of the two axes. We measured the real error of the FDSS; it was less than a 0.032 degrees, which FDSS requires.

Fig. 12, 13, 14, and 15 show the x-axis and y-axis error graphs with +45 degree rotation. The error value around zero degree in the Fig. 11 is increased because of the effect of the sunlight reflection in the optical system and CIS alignment. Because present anti- reflection techniques are imperfect, it is very difficult to align the CIS to the horizontal and vertical axes. Also the plane of the CIS surface is not uniform. But we did not compensate the errors by using the measurement algorithm.

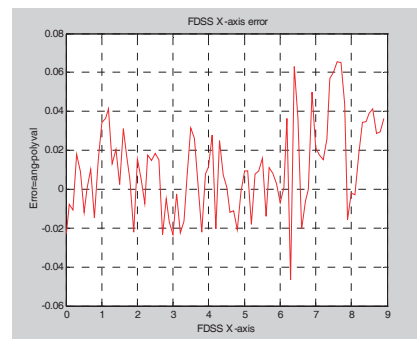


Fig. 13. FDSS +x-axis error result with +45 degree rotation.

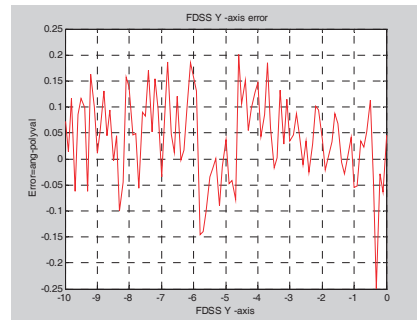


Fig. 14. FDSS -y-axis error result with +45degree rotation.

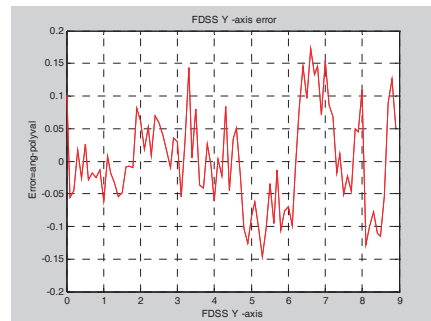


Fig. 15. FDSS +y-axis error result with +45degree rotation.

## 5. Conclusion

The incident characteristics of sunlight for the FDSS have been analyzed. After considering the results of the analysis and simulation, we designed, manufactured, tested, and calibrated the FDSS successfully.

The feasibility of the developed FDSS was verified by now. But the errors, which are affected by factors such as temperature, power characteristics and the Fixed Pattern Noise (FPN) of the CIS, and real measurement algorithm, were considered.

Especially, error compensations according to a certain range of angles were considered. Also the performance test of FDSS needs to be verified by an orbit test of the STSAT-2. On orbit the test can be tested by the star sensor which has with the accuracy less than 0.016degree.

Unfortunately, the performance mission of this FDSS could not be tested in orbit because of the two times launch failures of KSLV-1 (Korea Space Launch Vehicle-I).

## Acknowledgement

This work was supported by the STSAT-2 development project. The author also thanks the Power and Sensor team, the Attitude Determination and Control System team, and SI.

## References

- [1] Ok, G., Sun sensor manufacturing for Satellite on study, M.S. thesis, KAIST, Daejeon, South Korea, 1993, pp. 1-30.
- [2] Hales, J. H., and Pedersen, M., "Two-axes MOEMS Sun Sensor for Pico Satellites", *Proc. of the 16th Annual AIAAA/USU Conference on Small Satellites*, Logan, USA, 2002.
- [3] Hecht, Eugene, *Hecht Optics*, Addison-Wesley, New York, USA, 2000, pp. 585-615.
- [4] Yadid-Pecht, O., Pain B., Staller C., Clark C., and Fossum E., "CMOS Active Pixel Sensor Star Tracker with Regional Electronic Shutter", *IEEE Journal of Solid State Circuits*, Vol. 32, No. 2, 1997, pp. 285-288.
- [5] Wertz, J. R., *Spacecraft Attitude Determination and Control*, Kluwer Academic Publishers, Dordrecht, London, UK, 1988, pp. 221-230.
- [6] Clarke, T. A., Cooper, M. A. R., and Fryer, J. G., "An estimator for the random error in subpixel target location and its use in the bundle adjustment", *Optical 3D measurements techniques II*, Wichman, Karlsruhe, 1993, pp. 161-168.
- [7] Lason, W. J., and Wertz, J. R., *Space mission analysis and design 2nd edition*, , London, UK, 1992, pp. 360-363.